Electronic Supplementary Information

Au nanoparticle-decorated Ni$_2$P nanosheet arrays with porous grids for electroanalytical hydroquinone sensing

Wenbo Lu[*a], Xue Zhang[a], Wenting Tong[b], Ming Wei [*b]

a Key Laboratory of Magnetic Molecules and Magnetic Information Materials

(Ministry of Education), School of Chemistry and Material Science, Shanxi Normal

University, Taiyuan 030031, China.

b Kangda College of Nanjing Medical University, Lianyungang 222000, China

Corresponding author:

E-mail: luwb@sxnu.edu.cn ; weiming@njmu.edu.cn

Experimental

1. Reagents and materials

$Ni(NO_3)_2 \cdot 6H_2O$, CH_4N_2O and $AuCl_3 \cdot HCl \cdot 4H_2O$ were provided from Kemiou Chemical Reagent Co. Ltd. (Tianjin, China). NH_4F was obtained from Luoyang chemical reagent factory (Luoyang, China). NaH_2PO_2 was purchased from Guangfu Fine Chemical Research Institute (Tianjin, China). All reagents can be used directly without further purification.

2. Apparatus

Ultrapure water was obtained from a laboratory water purification system Eco-S15 (Hitech Instruments Co., Ltd., China). X-ray powder diffractometer (XRD) analysis was conducted using Ultima IV-185 diffractometer. Scanning electron microscopy (SEM) measurements were performed using JSM-7500F scanning electron microscopy. Transmission electron microscopy (TEM) and high-resolution TEM (HRTEM) images were obtained using FEI, tecnai F20 transmission electron microscopy. X-ray photoelectron spectroscopy (XPS) analysis was carried out using K-Alpha X-ray photoelectron spectrometer. Electrochemical characterization was conducted using an electrochemical workstation (CHI660E, Chenhua, China).

3. Optimization of differential pulse voltammetric parameters

In order to obtain maximum current response coupled with good discrimination from the background current and favorable peak shape, the influence of DPV operating parameters on HQ signal was examined before constructing the calibration curves.[1] The optimization of the DPV operating parameters was evaluated by either varying the modulation amplitude in the range of 10–80 mV (with a fixed pulse width of 50 ms) or the pulse width in the range of 10–80 ms (with a fixed modulation amplitude of 50 mV) for DPV (Fig. S1). It was found that higher values of modulation amplitude resulted in a remarkable improvement of HQ current response, and thus 50 mV was adopted due to the better defined peak with the highest peak current. On the other hand, the voltammetric signals of the analyte slightly decreased with an increase in pulse width. Therefore, a pulse width of 50 ms was selected as the most favorable option based on satisfactory peak current magnitude, high repeatability, and lower background.

4. Experimental setting of electrochemical measurements

Saturated Ag/AgCl, platinum sheet, and $Au/Ni_2P/NF$ (6 mm^2) are used as reference electrode, counter electrode, and working electrode, respectively. The CV measurements are performed in 5.0 mL PBS by scanning the potential from -0.1 to 0.4 V at the scan rate of 50 mV·s^{-1}. The DPV experiments are performed in 5.0 mL PBS from -0.1 to 0.4 V with pulse amplitude of 50 mV, pulse width of 50 ms, and pulse period of 500 ms. The amperometric experiments are performed in 5.0 mL PBS at the potential of 0.2 V with a sample interval of 0.1 s.
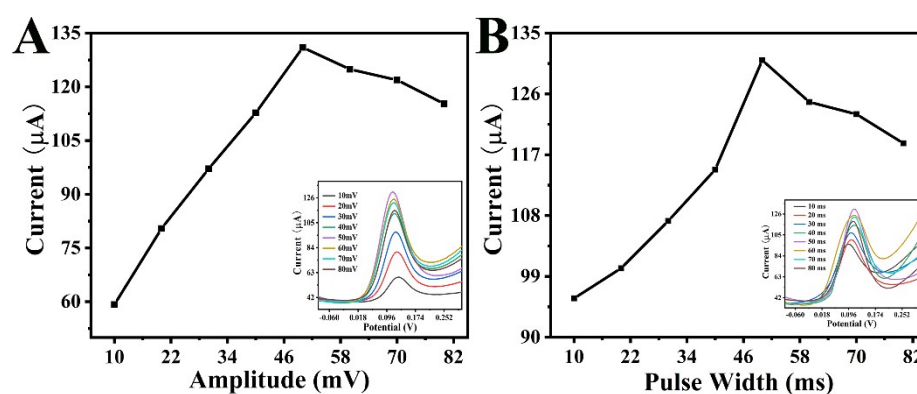

Fig. S1. DPV records for 1 mM HQ in PBS (0.1 M) solution on the $Au/Ni_2P/NF$ NSAs for (A) various modulation amplitudes; (B) various pulse widths.
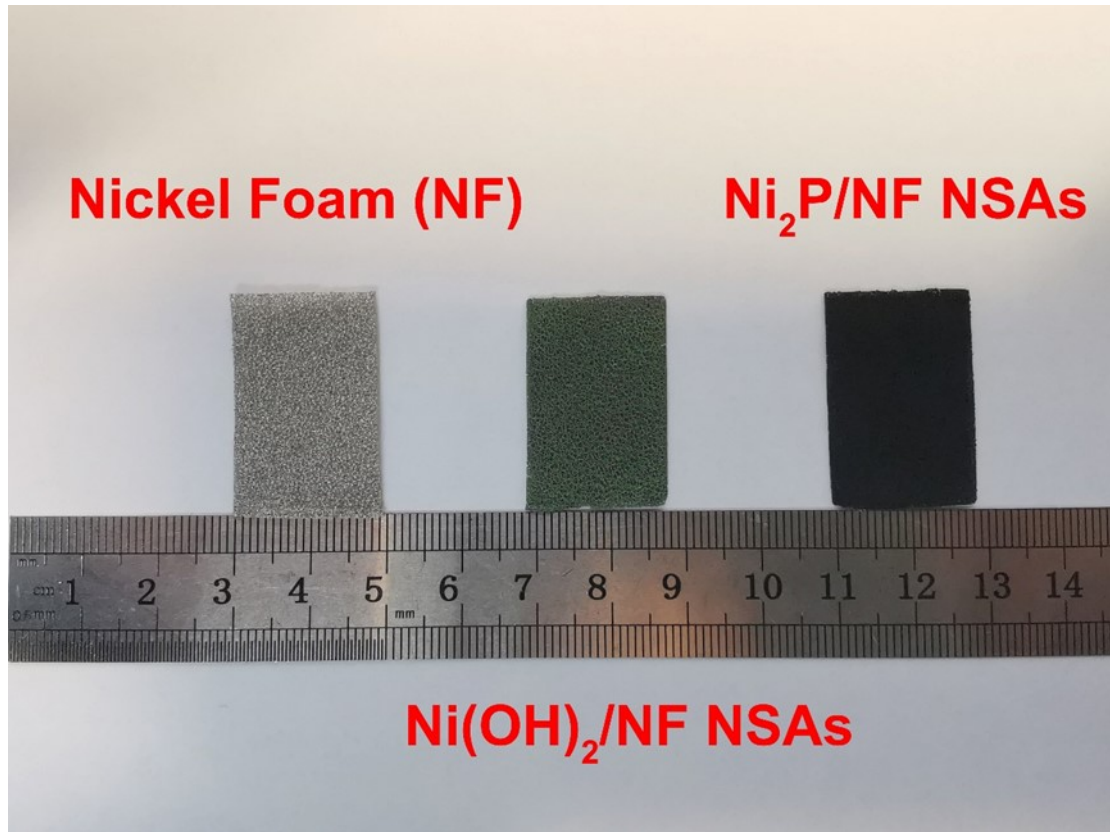
Fig. S2. Optical photographs of nickel foam, Ni(OH)$_2$/NF NSAs, Ni$_2$P/NF NSAs.
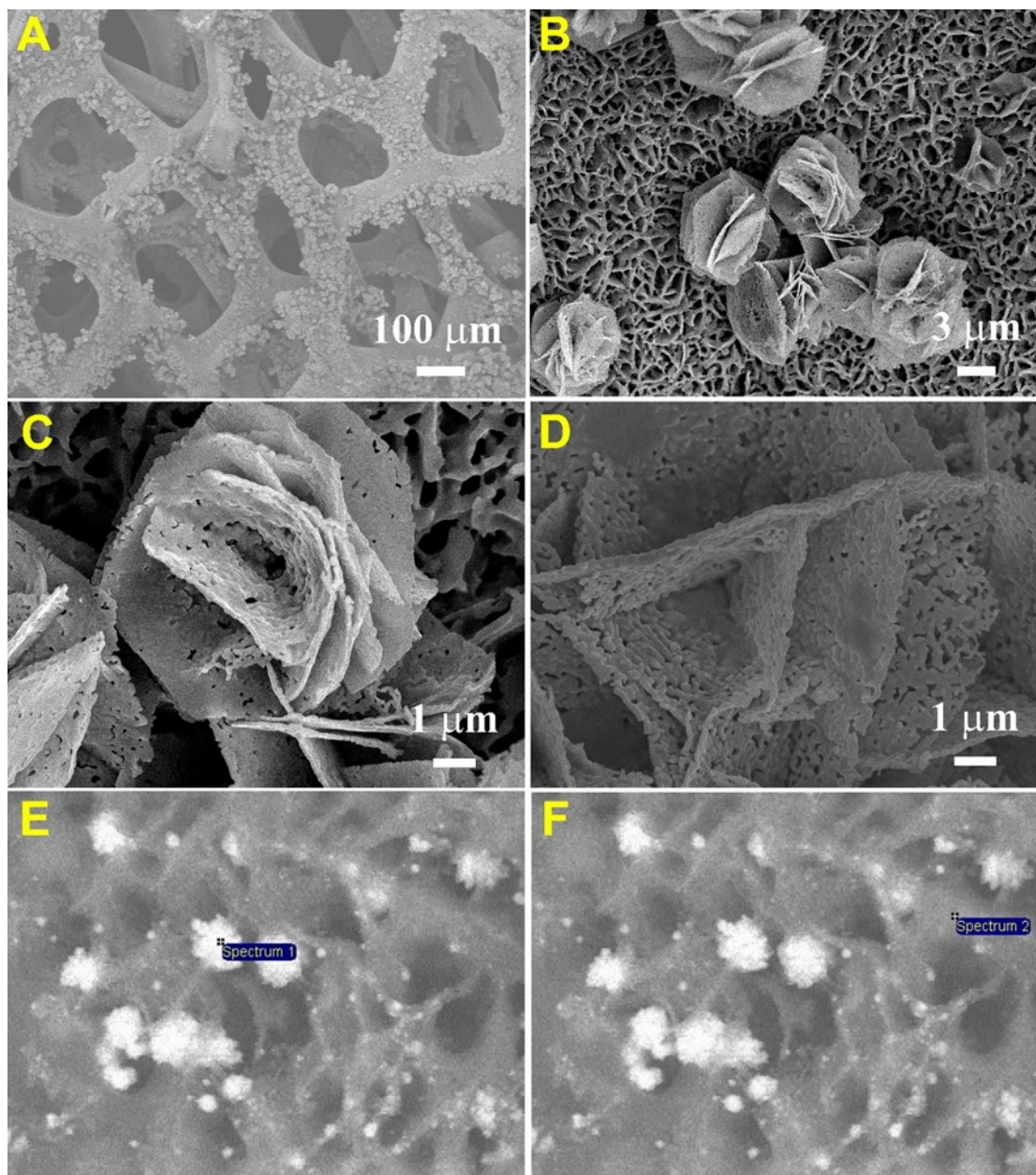
Fig. S3. (A) The SEM images of the modified electrode at low magnification; (B, C, D) SEM images of flake-flower Ni_2P architectures with porous grid at different magnifications; Backscattered electron imaging of $Au/Ni_2P/NF$ NSAs; (E) spectrum 1; (F) spectrum 2.
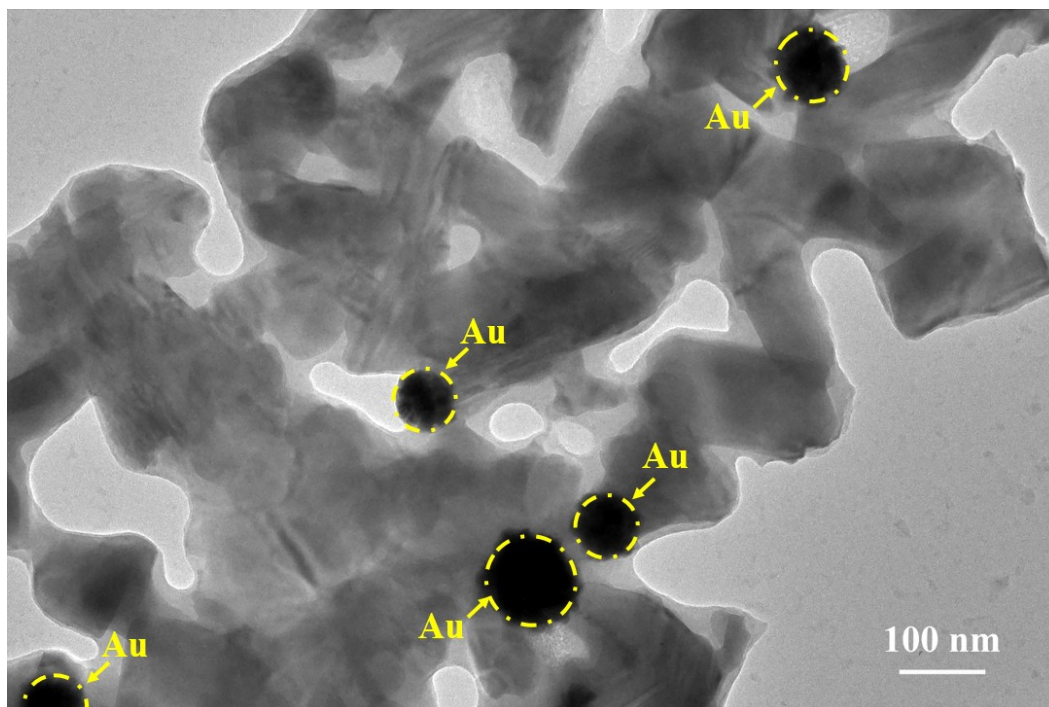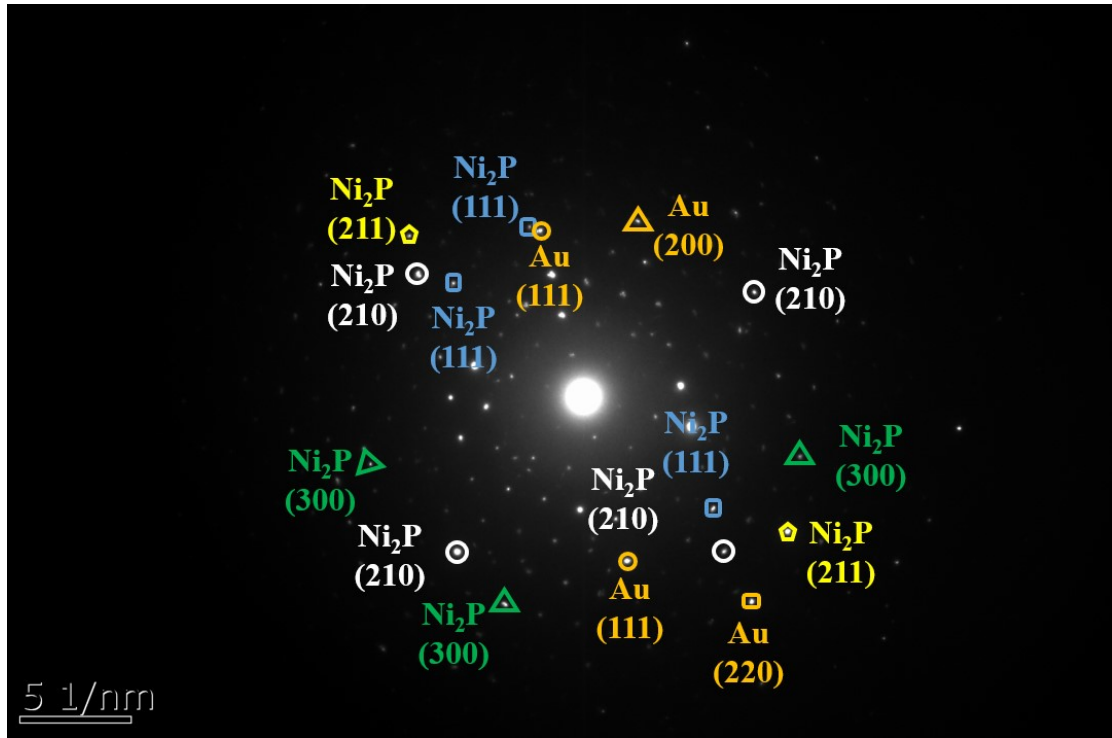
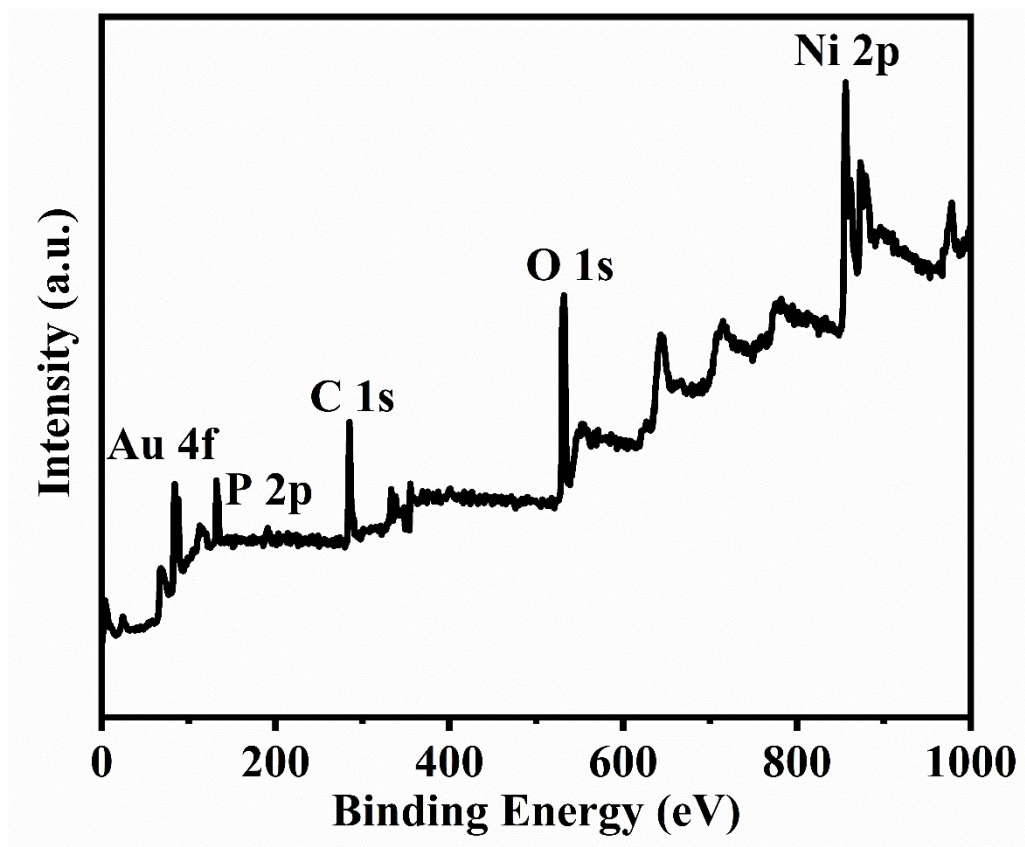**Fig. S4.** TEM image of Au/Ni$_2$P/NF NSAs.

Fig. S5. SAED pattern of Au/Ni$_2$P/NF NSAs.

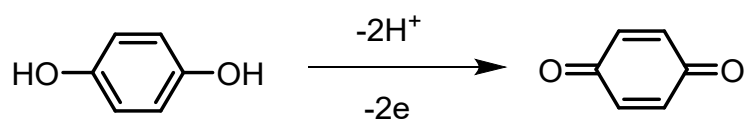**Fig. S6.** XPS survey spectrum of the Au/Ni$_2$P/NF NSAs.

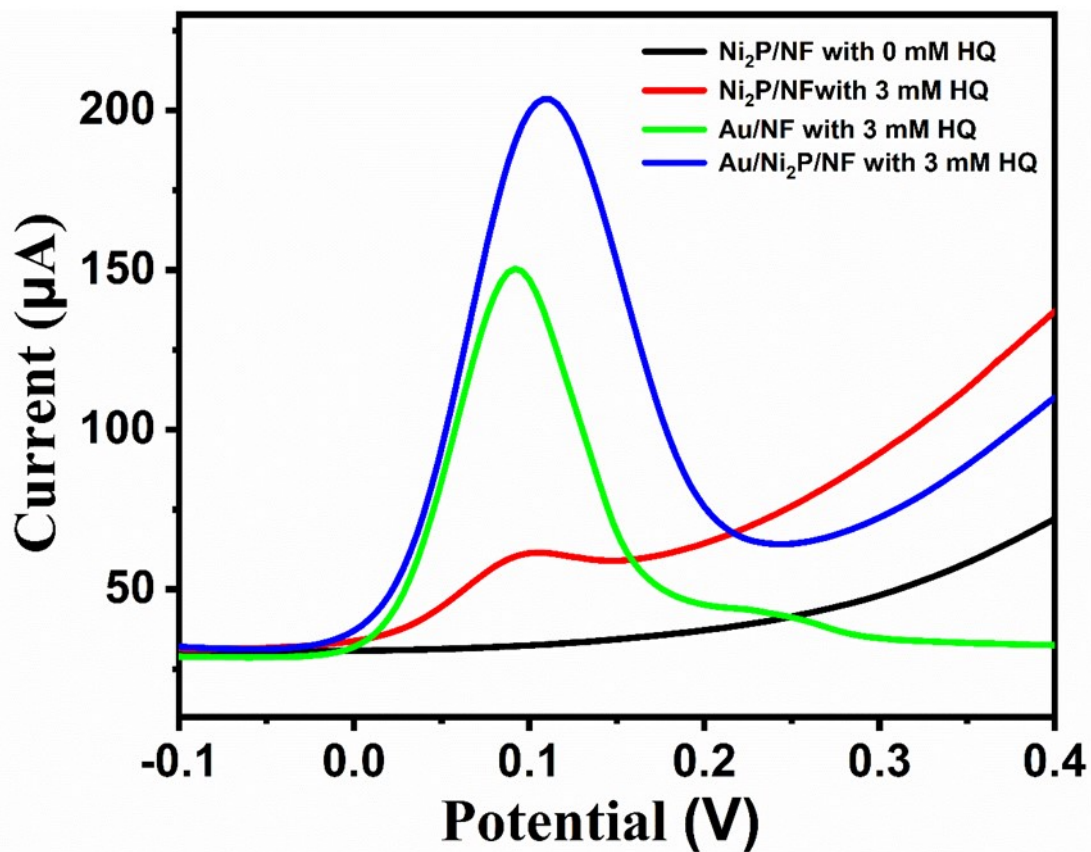**Fig. S7.** Redox mechanism of HQ at the Au/Ni$_2$P/NF NSAs.

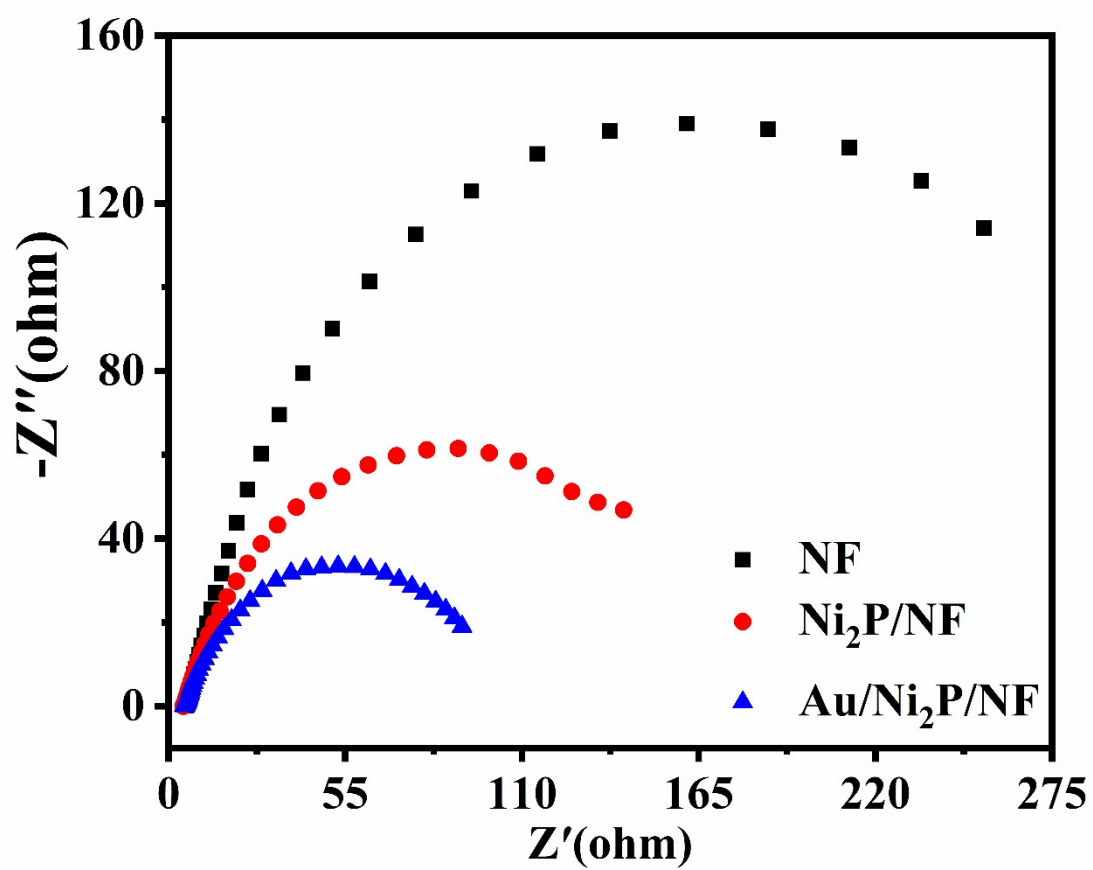**Fig. S8.** DPV response of Ni$_2$P/NF, Au/NF and Au/Ni$_2$P/NF in the presence of 3 mM HQ.

Fig. S9. EIS characterizations of bare NF, Ni$_2$P/NF and Au/Ni$_2$P/NF.

Table S1

Detailed binding energy calculation results

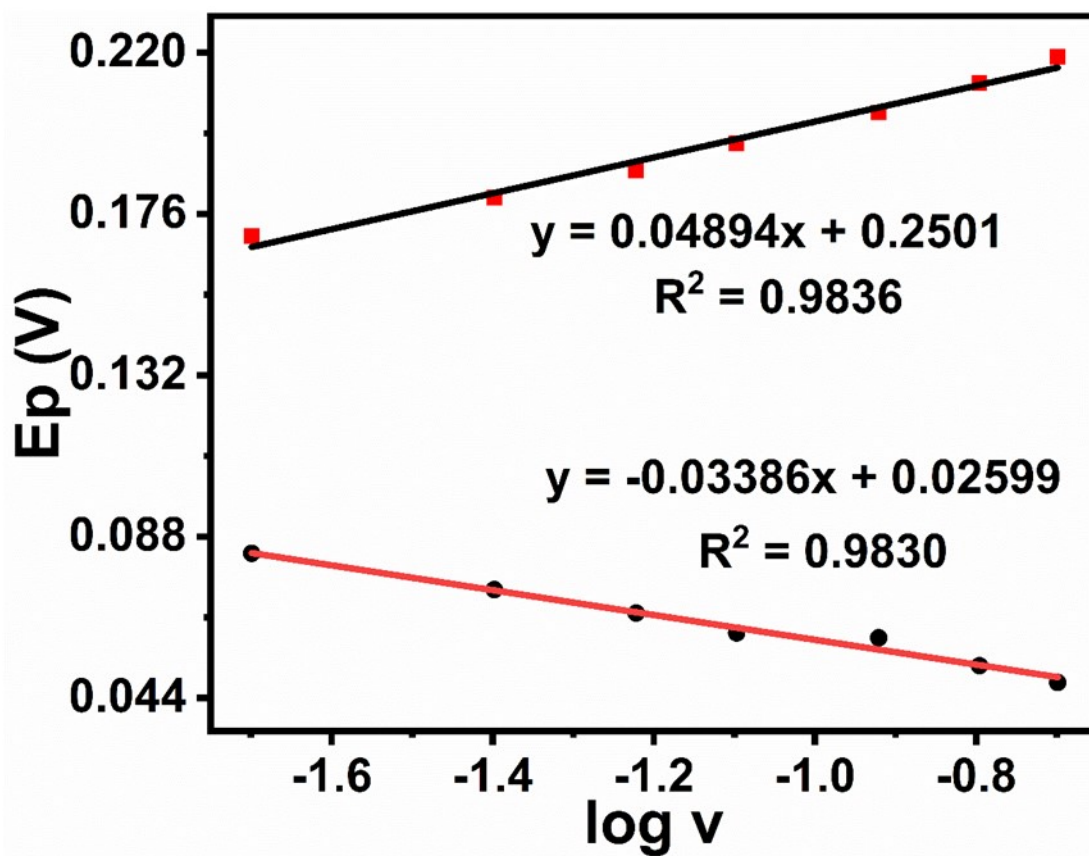| Systems	Energy (eV)	Binding Energy (eV)
HQ	-89.52622204	
BQ	-80.78294058	
Ni_2P	-202.4705141	
Ni_2P + HQ	-292.6594468	-0.66271065
Ni_2P + BQ	-284.495806	-1.24235133
Au/ Ni_2P	-200.2802447	
Au/Ni_2P + HQ	-290.6591821	-0.85271538
Au/Ni_2P + BQ	-282.1618319	-1.09864667

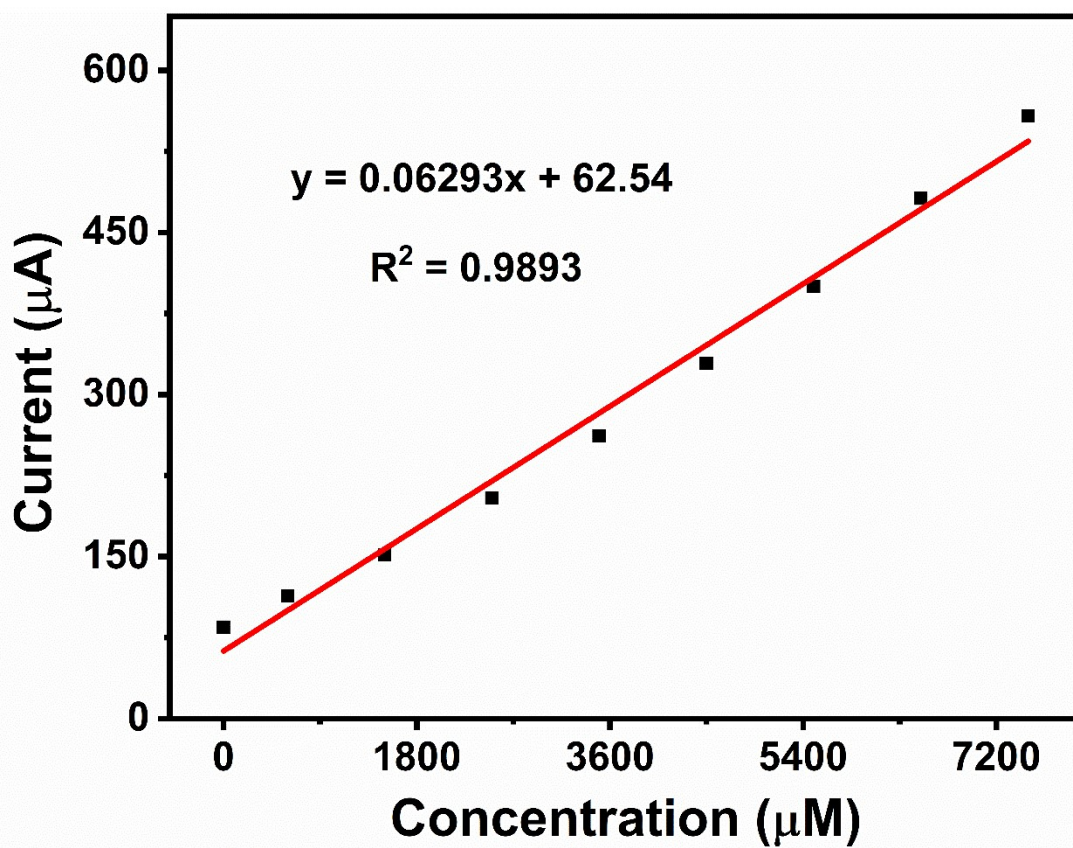**Fig. S10.** The linear relationship between the peak potential and the logarithm of scan rate.

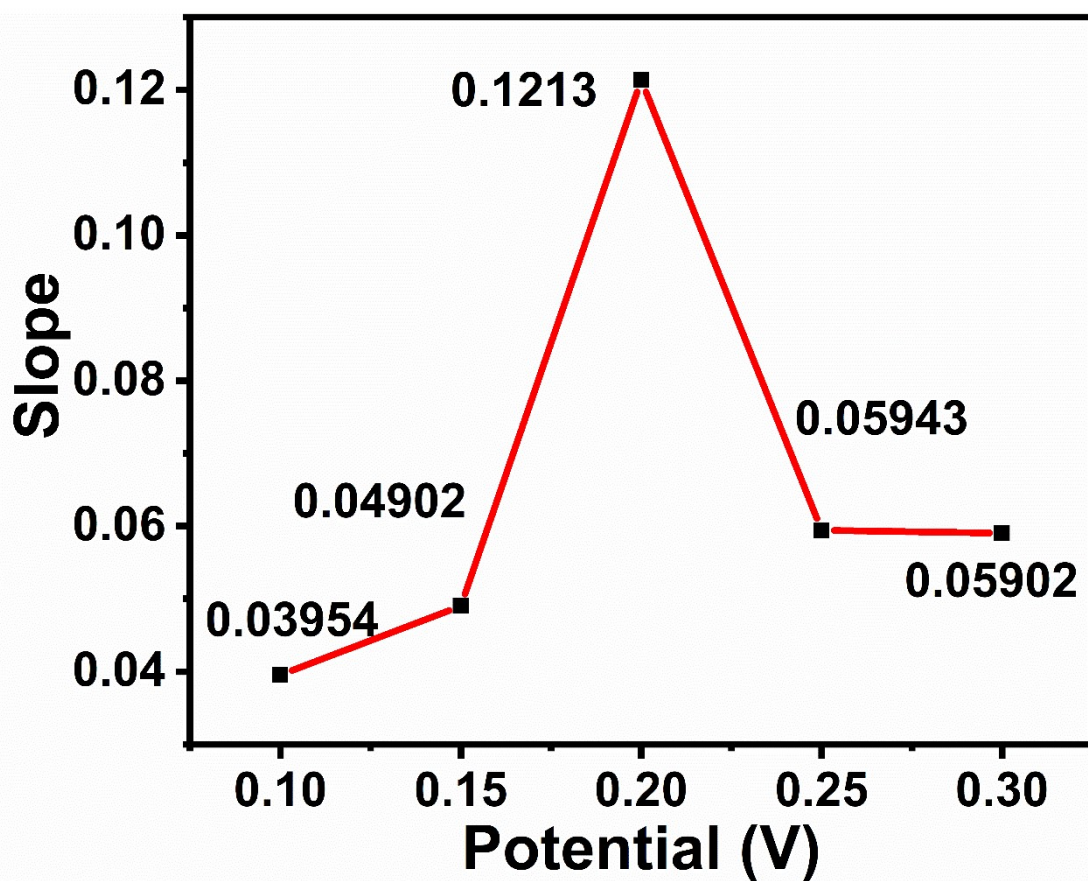**Fig. S11.** Calibration curve for the current response to HQ concentration.

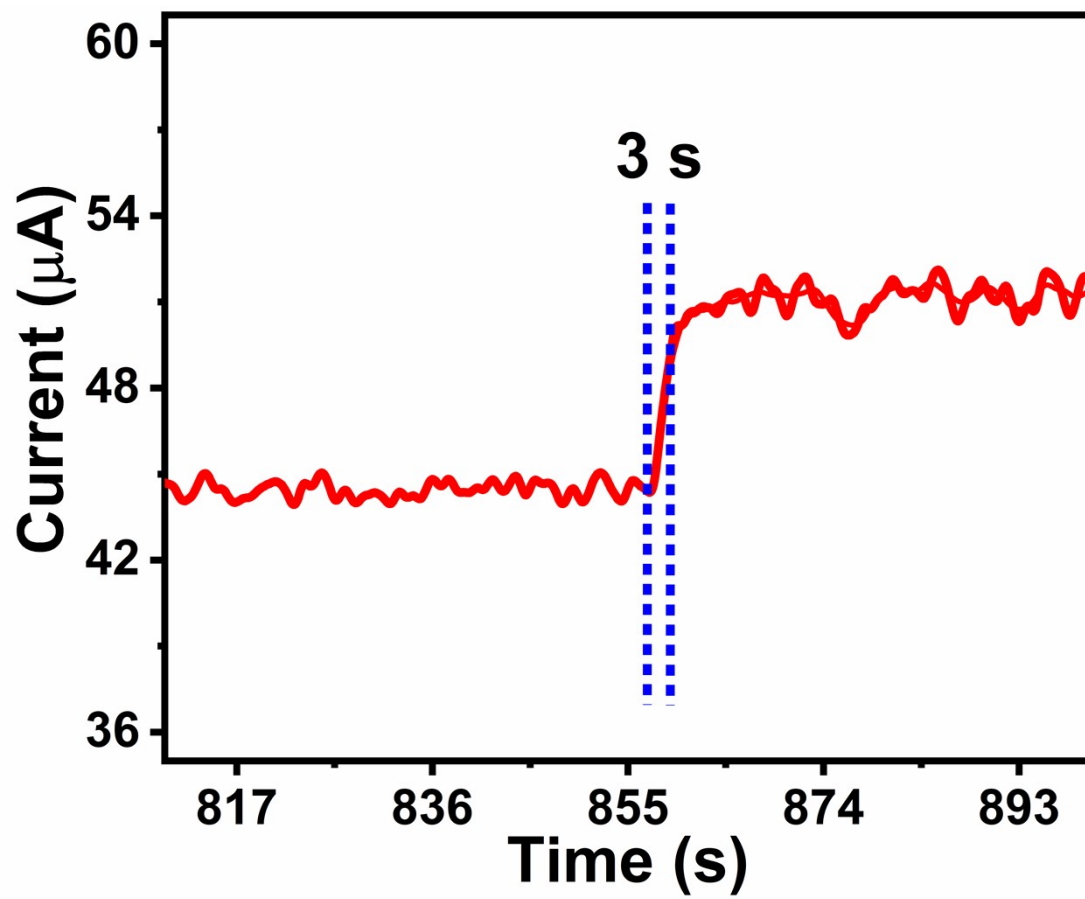**Fig. S12.** Line chart of the slopes at different working potentials.

Fig. S13. The response time curve of HQ oxidation.

Table S2

Comparison in performance of present HQ sensor with other reported electrochemical HQ sensors

| Electrodes	Linear range (μmol/L)	LOD (μmol/L)	Ref.
$Au_3@Pd_6$/GCE	4 ～ 5000	0.63	[2]
AuNPs/RGO/WO_3	0.1 ～ 10	0.036	[3]
rGO-Fe_3O_4-Au/GCE	0.1 ～ 500	0.17	[4]
Au-g-C3N$_4$	1.0 ～ 320	0.3	[5]
Co/poly-L-glu/GCE	3.85 ～ 1300	0.497	[6]
KOH-activated GSEC film	0.5 ～ 200	0.1	[7]
pDNPH/AGCE	20 ～ 250	0.75	[8]
MIL-101(Cr)-rGO-2-CPE	4 ～ 1000	0.66	[9]
CuS NCs/CS /GCE	4.5 ～ 4500	1.5	[10]
Fe_2O_3/CNTs/FTO	1 ～ 260	0.5	[11]
AuNPs/Fe_3O_4-APTES-GO	3 ～ 137	1.1	[12]
P4VPBA/PPy/GO	4 ～ 22	0.53	[13]
NiO/CNT	10 ～ 500	2.5	[14]
Au-Pd NF/rGO/GCE	1.6 ～ 100	0.5	[15]
Au/Ni_2P/NF NSAs	0.5 ～ 4000	0.26	This work
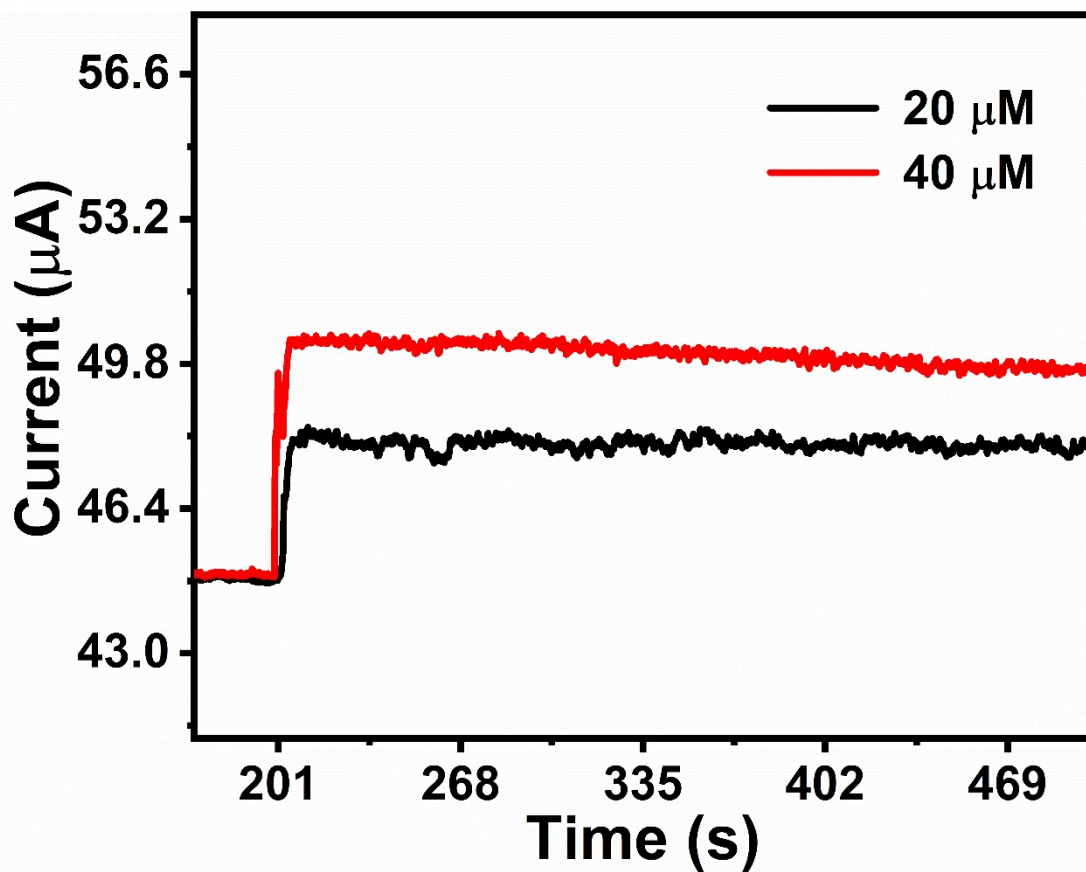
Fig. S14. Chronoamperogram of the current behavior after HQ addition for 350 s.
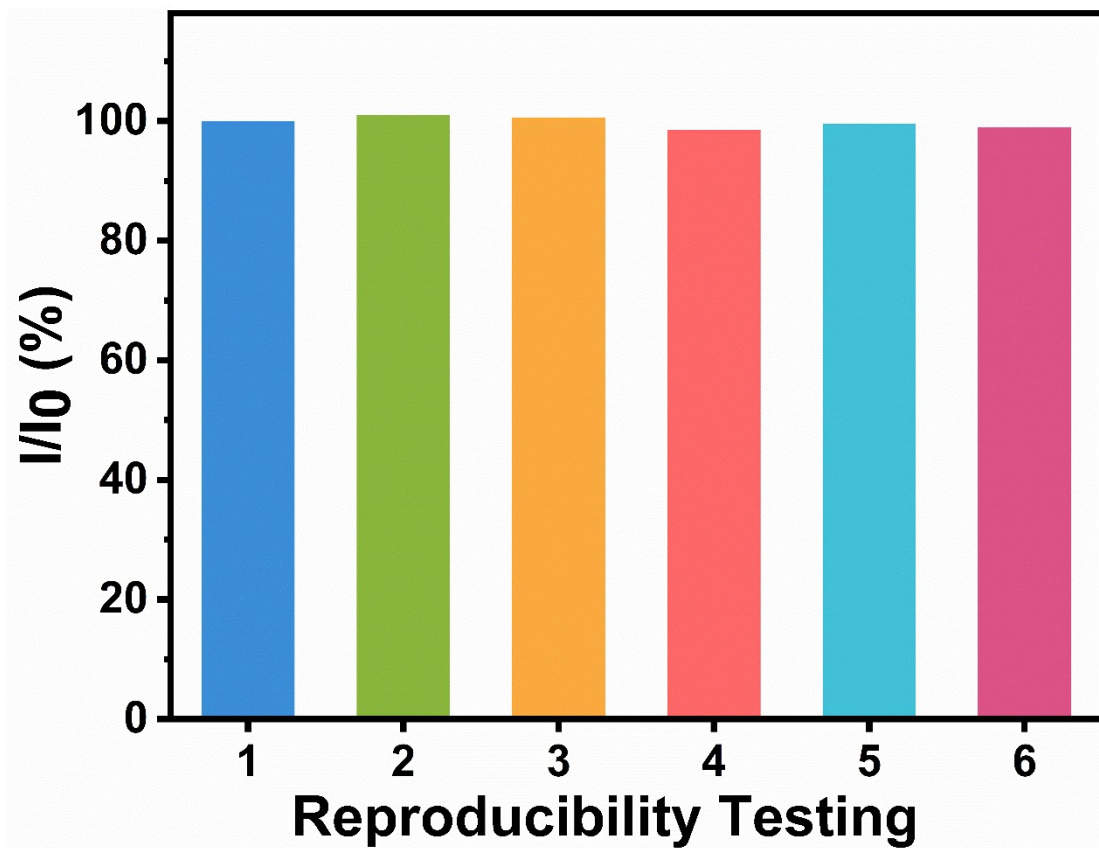
Fig. S15. Reproducibility of 6 sensors towards 1 mM HQ in 0.1 M PBS.

Reference：

[1] O. Sarakhman, L. Dubenska, L, Švorc, J. Electroanal. Chem., 2020, **858**, 113759.

[2] T. Chen, J. Xu, M. Arsalan, Q. Sheng, J. Zheng, W. Cao, T. Yue, *Talanta,* 2019, **198**, 78-85.

[3] M.-S. Tsai, C.-J. Lu, P.-G. Su, *Mater. Chem. Phys.,* 2018, **215**, 293-298.

[4] F.-Y. Kong, R.-F. Li, L. Yao, Z.-X. Wang, H.-Y. Li, W.-X. Lv, W. Wang, *Microchim. Acta,* 2019, **186**, 177.

[5] H. Guo, Y. Shen, H. Ouyang, Y. Long, W. Li, *Microchim. Acta,* 2019, **186**, 819.

[6] B. Huang, C. Yao, J. Yang, S. Du, X. Lu, *RSC Adv.,* 2020, **10**, 43834-43839.

[7] L. Huang, Y. Cao, D. Diao, *Sens. Actuators B Chem.,* 2020, **305**, 127495.

[8] N. S. Lopa, M. M. Rahman, H. Jang, S. C. Sutradhar, F. Ahmed, T. Ryu, W. Kim, *Microchim. Acta,* 2017, **185**, 23.

[9] H. Wang, Q. Hu, Y. Meng, Z. Jin, Z. Fang, Q. Fu, W. Gao, L. Xu, Y. Song, F. Lu, *J. Hazard. Mater.,* 2018, **353**, 151-157.

[10] J. Zou, J. Ma, Y. Zhang, L. Huang, Q. Wan, *J. Chem. Technol. Biotechnol.,* 2014, **89**, 259-264.

[11] Y. Liu, H. Liao, Y. Zhou, Y. Du, C. Wei, J. Zhao, S. Sun, J. S. C. Loo, Z. J. Xu, *Electrochim. Acta,* N 2015, **180**, 1059-1067.

[12] S. Erogul, S. Z. Bas, M. Ozmen, S. Yildiz, *Electrochim. Acta,* 2015, **186**, 302-313.

[13] H. Mao, M. Liu, Z. Cao, C. Ji, Y. Sun, D. Liu, S. Wu, Y. Zhang, X.-M. Song, *Appl. Surf. Sci.,* 2017, **420**, 594-605.

[14] L. Zhao, J. Yu, S. Yue, L. Zhang, Z. Wang, P. Guo, Q. Liu, *J. Electroanal. Chem.,* 2018, **808**, 245-251.

[15] Y. Chen, X. Liu, S. Zhang, L. Yang, M. Liu, Y. Zhang, S. Yao, *Electrochim. Acta,* 2017, **231**, 677-685.